Collisional angular-momentum mixing of Na Rydberg states with Xe

R. Kachru, T. F. Gallagher, F. Gounand,* K. A. Safinya,† and W. Sandner‡
Molecular Physics Laboratory, SRI International, Menlo Park, California 94025
(Received 8 March 1982)

The collisional angular-momentum mixing of the Na nd Rydberg states into states of higher angular momentum with Xe as the collisional partner has been studied in zero field and in the presence of a small electric field. The collisional l-mixing cross section in zero field has been measured for $9 \leq n \leq 23$ using a vapor-cell-fluorescence method and a crossed-beam technique with a selective-field-ionization (SFI) scheme as the state detector. Using the $|m_l|$ selectivity of the SFI, we have also investigated the final-$|m_l|$-state distribution of the collisionally populated states of $l > 2$. Our measurements suggest that the collisionally populated states have predominantly low $|m_l|$ values ($|m_l| \leq 2$). An application of a low electric field (~ 50 V/cm) substantially reduces the collisional population of the low-$|m_l|$ states, thus reducing the total cross section as well.

I. INTRODUCTION

Collisional l mixing of highly excited Rydberg states has recently attracted considerable interest both experimentally as well as theoretically.[1–10] In particular, exhaustive studies of the l-mixing cross section of the Na d and f states, i.e., the collisional redistribution of an initially excited n,l state to nearly degenerate states of higher l but same n have been reported. These experiments were carried out in a field-free environment. It is, however, well known that the highly excited Rydberg atoms can be easily distorted by relatively small electric fields, which are present in many situations where such collision processes are important (plasma physics, astrophysics, etc.). It is therefore of some interest to study the effect of a small electric field on the l-mixing process involving the Rydberg atom and the perturber, and preliminary reports of such studies have appeared.[11]

Previous measurements of the noble-gas-induced collisional redistribution of the Na nd states into states of higher angular momentum l have revealed that these cross sections are quite large (peak values of 4000 Å^2).[1] For all the noble gases used as collisional partner—He, Ne, and Ar—the collisional-mixing cross section $\sigma_{l\text{mix}}$ increases rapidly as n (the principal quantum number) increases from 5 to 10 and then slowly decreases at higher n. Here we report measurements that were made on the nd state of Na with Xe as a collision partner. Using an atomic beam with selective-field-ionization (SFI) detection and a vapor cell with time-resolved fluorescence detection method, we have measured the Xe-induced l-mixing cross section $\sigma_{l\text{mix}}$. Furthermore, the use of the SFI technique has the potential of revealing additional information about the collisional redistribution process. In particular, the well-known selectivity of the field-ionization process on the binding energy of the state[12] and its $|m_l|$ can be used to study the $|m_l|$ and l distribution of the collisionally distributed $l > 2$ states of the atoms.[13] Our measurements indicate that the collisional redistribution process results in approximately equal populations of low- ($0 \leq |m_l| \leq 2$) and high-$|m_l|$ states. In addition, the low-$|m_l|$ states are clearly equally distributed over the $l > 2$ states. Similar measurements in the presence of a small electric field indicate that the electric field alters the cross section $\sigma_{l\text{mix}}$ as well as the final-state distribution, particularly of the low-$|m_l|$ states.

The choice of Xe as a collisional partner for the electric field experiments was dictated by the fact that many of our measurements were done in a Na beam apparatus, using SFI as the state detector. The large $\sigma_{l\text{mix}}$ with Xe (about eight times larger than Ar) provided us with large collisional-mixing rates, at relatively low Xe pressure ($< 10^{-4}$ Torr). As the first part of the experiment, the l-mixing cross section $\sigma_{l\text{mix}}$ was determined for n ranging from 9 to 23, in a zero-field environment. For $n \leq 15$ we used a cell-type apparatus, described in Ref. 1, with a time-resolved fluorescence technique to determine the absolute cross section. In addition to mapping out the range of n over which the maximum change in $\sigma_{l\text{mix}}$ occurs, the cell measurements provide a means of normalizing to an absolute cross section the relative cross sections obtained at high n values using a beam apparatus and SFI. For $n \geq 15$ a crossed atomic beam approach employing SFI was used to obtain relative cross sections which were then assigned absolute values by normalizing at $n = 15$ to the cell data. Using the beam apparatus

and SFI detection we then explored the final-state distributions and the effects of small electric fields.

II. EXPERIMENT

A. Cell experiment

The basic approach for measuring the collisional redistribution rates using the time-resolved fluorescence technique is shown in Fig. 1. The Na atoms are excited from the $3s_{1/2}$ ground state to the nd excited states by two successive dye-laser pulses resonant with the $3s$-$3p_{3/2}$ and $3p_{3/2}$-nd transitions, respectively. The time-resolved fluorescence from the Na $nd \rightarrow 3p$ transition exhibits a rapid decay followed by slower decay.[1] The fast decay rate k_+ is given by $k_+ = k_r + A_d$, where A_d is the pressure-independent radiative decay rate of the d state,[14] and k_r, the collisional-mixing rate, represents the loss of population in the d states due to collisions which transfer atoms into nearby states of $l > 2$, e.g., f,g,h states. The pressure-independent slow decay rate k_-, as manifested by the slower decay, represents the average lifetime of the $l \geq 2$ states, since the population can be transferred from $l > 2$ states back to the d state. The time-dependent $nd \rightarrow 3p$ fluorescence (at a fixed perturber pressure) can therefore be fit to a sum of two exponentially decaying rates. The fast exponential rate can be related to the l-mixing cross section by

$$\sigma_{l\text{mix}} = k_r / n V_r ,$$

where n is the perturber number density,

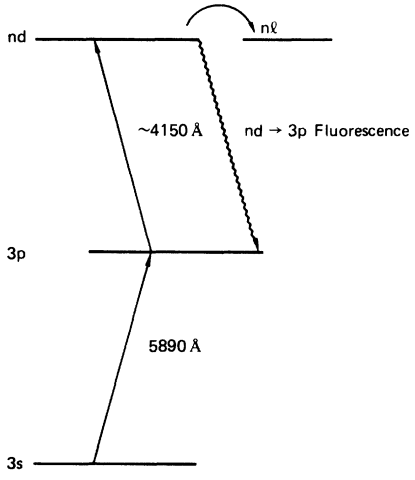

FIG. 1. Schematic of the collisional angular-momentum mixing of the Na nd states in a vapor-cell apparatus. A selected nd state is pumped by two dye-laser pulses. The collisional redistribution to the higher-l states is detected by monitoring the population in the nd state by detecting the $nd \rightarrow 3p$ fluorescence.

$$V_r = (8kT/\pi\mu)^{1/2}$$

is the average relative speed, k is Boltzmann's constant, T is the absolute temperature, and μ is the reduced mass.

Two grating-tuned dye lasers of Hansch design are pumped by the harmonics of a Quanta Ray Nd:YAG laser operating at 10 Hz. The 5-ns-long dye-laser pulses with 20 GHz linewidth full width at half maximum (FWHM) have typical energies of ~ 50 μJ per pulse. The first dye-laser beam pumps the $3s$-$3p_{3/2}$ ($\lambda = 5890$ Å) transition of Na, while the second dye-laser beam pumps the $3p_{3/2}$-nd transition. A 5-ns delay in the second dye-laser beam ensures that the $3p$ state is populated when it arrives in the cell. The two laser beams cross at an angle of $\sim 1°$ in a Pyrex cell which contains the Na and is heated to about 150 °C. The xenon pressure inside the cell is read by an MKS baratron capacitance manometer. The $nd \rightarrow 3p$ fluorescence signal is detected by a photomultiplier tube (PMT) in the direction perpendicular to the laser beam. Cutoff filters placed between the cell and the PMT greatly reduce the $3p \rightarrow 3s$ background fluorescence, while leaving the $nd \rightarrow 3p$ fluorescence light practically unattenuated. An EMI PMT gated to open 300 ns after the laser pulses is used to measure the time-resolved signal which is averaged with a Princeton Applied Research (PAR) box-car averager and recorded by a Digital Equipment Corporation PDP-11/40 computer for subsequent analysis. This procedure is used to determine $\sigma_{l\text{mix}}$ for d state with low n ($9 \leq n \leq 15$).

B. Beam experiment

Measurement of states with $n \geq 15$ are done using the crossed-beam approach. A schematic of our experimental set up is shown in Fig. 2. Sodium atoms in a beam apparatus are excited by two laser beams at right angles to the atomic beam. SFI, which has already proven to be a sensitive and efficient method of detecting Rydberg atoms, is used as a detector of the Na Rydberg states. This enables us to follow the evolution of atoms from the initial states (d states) to other states as a result of collisions with Xe.

Since SFI plays such an important role in these experiments, let us digress for a moment to review the field ionization of Na by pulsed electric fields with rise times of ~ 0.3 μs.[13] To do so it is first convenient to define three field regimes. Low fields are those for which the Stark effect is less than the fine structure or spin-orbit splitting. Intermediate fields are such that the Stark effect is larger than the fine-structure interactions but smaller than the term separation Δn. High fields are those for which the Stark effect is larger than the Δn separation. As the

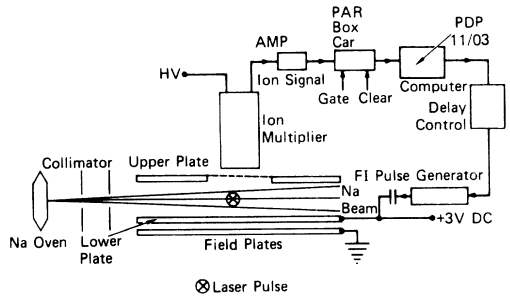

FIG. 2. Experimental setup for collision l mixing in a crossed-beam apparatus. The two dye-laser pulses which pump the nd state cross the Na beam emanating from an effusive Na oven at right angles between the field plates. A 0.3-μs-rise-time field-ionizing pulse ionizes the atoms and pushes the ions through a mesh into an electron mutliplier. A dc field (if required) is applied to the lower plate and the upper plate is normally grounded. The delay between the laser and the FI pulse is controlled by a PDP-11/03 computer which also records the ion signal via the gated box-car averager (PAR 160) operated in a linear mode.

field ionization pulse is applied, an Na atom excited in a low-field state with good quantum numbers L,S,J,m_j passes adiabatically with respect to m_j to an intermediate field regime where L,S,m_l,m_s are the good quantum numbers. The atom then passes adiabatically with respect to m_l through the high-field regime to the ionizing field (the spin is unimportant), and ionization occurs at the threshold field E_T required classically for ionization. For $|m_l|=0$ states

$$E_T = 1/(16n_s^4) ,$$

where n_s, the effective quantum number in the field, is defined by the binding energy W relative to the zero-field ionization limit in the field;

$$W = -1/(2n_s^2) .$$

Owing to a centrifugal barrier for $|m_l| \neq 0$ states, E_T is slight higher for them and increases with $|m_l|$.[13]

Using this model of field ionization let us consider an experiment in which we populate all the $|m_j|$ levels of an $nd_{5/2}$ level and immediately thereafter ionize them with an electric field. We expect to see three sharp steps in the ionization current, at the threshold fields for ionization of the three $|m_l|$ states, as we raise the amplitude of the ionizing pulse. These are shown schematically in Fig. 3. For $n \geq 18$ the $|m_l|=2$ state no longer pass from intermediate to high field adiabatically but begin to exhibit partially diabatic ionization leading to multiple thresholds at fields higher than the sharp step labeled $|m_l|=2$ in Fig. 3.

Since the collisional process leads to the population of states with the same n (as the d state) but with $l>2$, it is important to understand where the field-ionization thresholds of these states lie. While the exact l dependence of the threshold field for these manifold states ($l>2$ states) is complicated, it has been shown that for a given $|m_l|$, the threshold for the field ionization decreases as l increases[13] if the passage from the low to high field occurs adiabatically. This is illustrated in Fig. 3, where the range of the field-ionization thresholds for the d states is sketched. For instance, the region just below the $|m_l|=0$ threshold for the d state, indicated by the "0" bracket in the diagram, corresponds to the electric field range over which $l>2$ states with $|m_l|=0$ ionize. Note that the highest-l states ionize at the lowest field and the lowest-l state ($l=2$) at the highest field. Similarly, $l>2$ states with $|m_l|=1$ and 2 field ionize in the range indicated by the "1" and "2" brackets in the diagram.

Thus far we have considered only the adiabatic ionization of the low-$|m_l|$ states. The $|m_l|>2$ state ionize by following a diabatic passage with respect to $|m_l|$ from intermediate to high field and are expected to ionize at fields roughly twice the adiabatic thresholds.[13,15] It is, of course, impossible to directly excite such states with two lasers. To check this prediction, however, the expected thresholds for diabatic field ionization may be calculated from a hydrogenic model and are in good agreement with a previous observation of field ionization of the final-state distribution following collisions of Na nd states with Xe. In this work we do not attempt to resolve the details of the observed diabatic ionization signals but simply label such signals as resulting from $|m_l|>2$ states. Finally, it is important to note that in the range of n studied here, the $|m_l|=2$ states change from totally adiabatic ionization to partially diabatic ionization at $18d$.[13] The diabatic ionization leads to multiple $|m_l|=2$ thresholds in the region

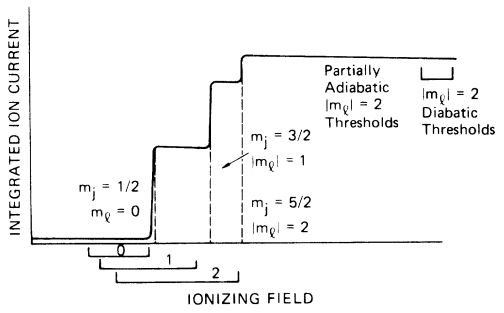

FIG. 3. Sketch of the threshold ionization behavior of the Na nd and higher angular-momentum states (see text).

between the $|m_l| = 2$ threshold and the diabatic ionization threshold of Fig. 3.

In our present experiment atoms are initially excited to the d state in low fields (a small field of 3 V/cm to define the quantization axis is always present in our experiment), where $|m_j|$ is a good quantum number. The two dye-laser beams are polarized parallel to the electric field quantization axis. This choice of laser polarization leads to the $\Delta m = 0$ selection rule and precludes excitation of the $|m_j| = \frac{5}{2}$ substate. Therefore in the absence of any collisions only the $|m_l| = 0$ and 1 thresholds appear in the field-ionization (FI) spectrum, as shown by Fig. 4(a).

In the present experiment we extensively use the plot of the ion current as the FI pulse amplitude is increased (see, for example, Fig. 4) to infer the population of the various final $n,l,|m_l|$ states, by using the FI threshold properties of these states. To avoid repeating this crucial connection between the ion current plot and the state distribution, we simply refer to the ion-current plot as the final-state distribution throughout this paper. However, it should be borne in mind that the plots such as Fig. 4 are in fact field-ionization plots from which we infer final-state distributions. The collisional redistribution of the initially excited states into states of $l > 2$, resulting from the introduction of the Xe into the Na beam, is shown in Fig. 4 for $n = 18$. Figure 4 shows the plot of ion current as the ionizing-field-pulse amplitude is increased for several delay times τ between excitation and field ionization. In Fig. 4(a), $\tau = 1$ μs, and the amount of collisional redistribution is small. The abrupt increase in the ion

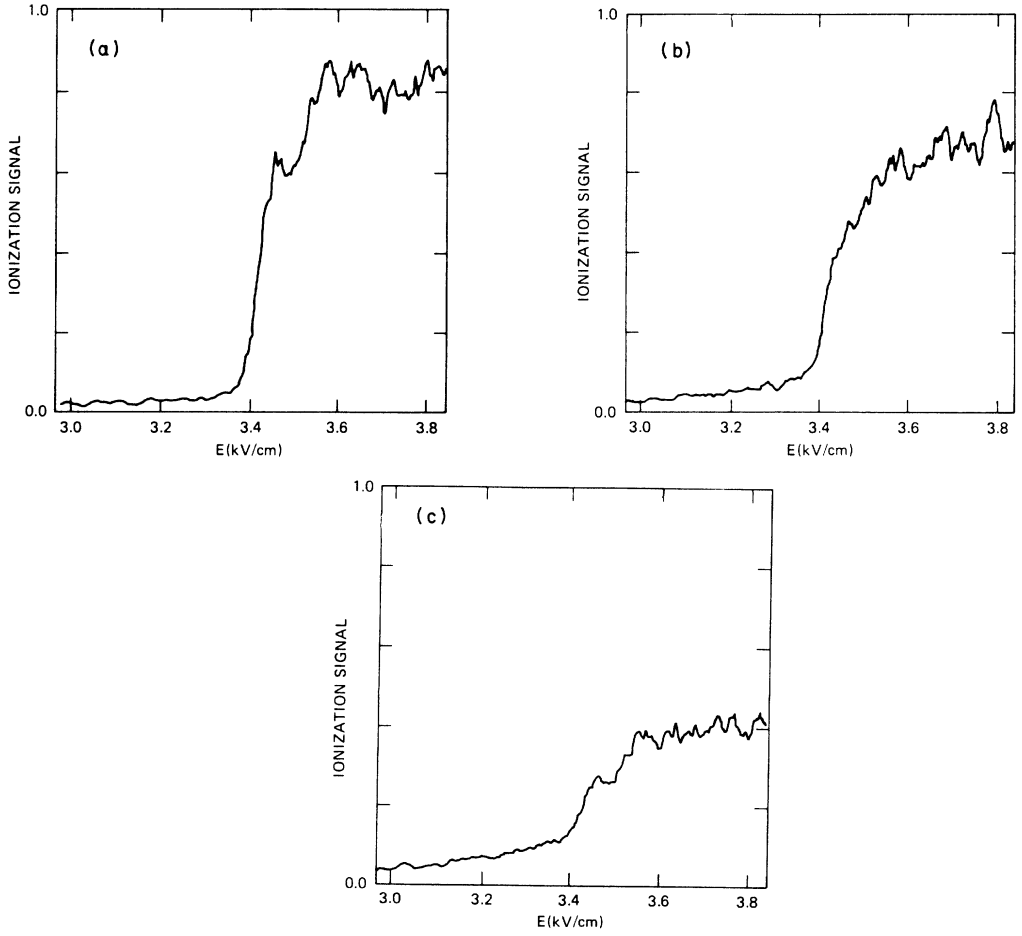

FIG. 4. Plot of the ion current as the field-ionization voltage is increased at a fixed Xe number density. The two thresholds at 3.4 and 3.5 V/cm correspond to the Na $18d_{5/2}$, $|m_j| = \frac{3}{2}$ and $\frac{1}{2}$ states. The amount of collisional redistribution increases from plots (a) to (c) as the time delay between the FI pulse and the laser pulses is increased from 1 to 3 μs. All the plots have the same relative scale. Note that the base line increases as τ is increased from 1 to 3 μs, reflecting the increase in the blackbody-radiation–induced transition rate from the initially excited $15d_{5/2}$ state to the nearby states (see Ref. 14).

current, i.e., the steplike features in the ion current at two distinct fields, shows the population present in the $18d$, $|m_l|=0$ and 1 states, respectively, at $\tau=1$ μs after the laser-pulse excitation. The collisional redistribution becomes evident in Fig. 4(b) where $\tau=2$ μs. Two important changes now emerge: (a) the height of two sharp step features is reduced, and (b) a collision signal with no sharp threshold, beginning at a field just below the $|m_l|=0$ threshold of the d state appears everywhere. Figure 4(c) shows a further increase in the collision signal and reduction of the sharp steps as τ is increased to 3 μs. From Fig. 4 it is evident that the reduction in the sharp threshold signal reflects the number of Na atoms lost from the d state, either by radiative decay or through the collisional redistribution process and that the appearance of the continuously increasing ionization signal superimposed on the sharp features represents the collisionally populated $l>2$ states.

Using the fact that field ionization of the d states shows up as two sharp steps in the ion current, we can monitor the population decay of the d state by measuring the decay of this steplike feature. Experimentally, the decay of the $|m_l|=0$ component of the d state, measured as τ, is increased (at fixed Xe pressure), first with the ionizing-field-pulse amplitude set just above the threshold and then set just below the threshold. The difference in these two decay signals then gives the temporal decay of the d-state population. The time-resolved decay of the $|m_l|=0$ component of the d state is similar to the time-resolved fluorescence of the $nd\rightarrow 3p$ transition.[1] The decay can fit to a sum of a fast and a slow exponential decay rate. The fast decay rate $k_+=k_r+A_d$, where A_d and k_r are the radiative and collisional decay rates of the d state, respectively.

An atomic beam of Na atoms passes between a plate and a grid, separated by 1.12 cm. Two dye-laser beams, tuned to the Na $3s$-$3p_{3/2}$ and $3p_{3/2}$-nd transitions across the Na beam between the plate and the grid at right angles. At a variable time τ subsequent to the laser pulses a high-voltage pulse of 0.3 μs rise time is applied to the lower plate, field ionizing the Rydberg states and accelerating the ions that are formed through the grid into an electron multiplier (as shown in Fig. 2). Xenon gas is introduced into the interaction region via a hypodermic syringe needle. The xenon pressure drop across the needle is $\sim 10^4$, and the pressure on the high-pressure end is regulated by a needle valve and monitored by an MKS capacitance manometer. The time delay τ between the laser pulses and the ionizer pulse is generated by a delay module which is controlled by a PDP-11/03 computer. A typical run, shown in Fig. 5, consists of varying τ in the range of

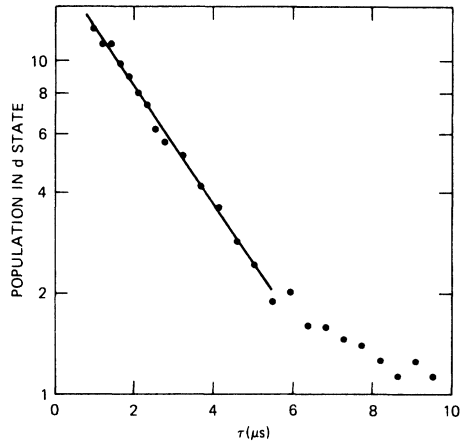

FIG. 5. Measured decay of $18d$ ($|m|=0$) state of Na as a function of time. The Xe number density is kept fixed during this run. Each point shown above represents the ion signal from the $18d$ state averaged over 100 laser shots. The data was automatically recorded by a PDP-11/03 computer.

1–10 μs in increments of 50–500 ns at a fixed xenon pressure. Each point in a typical run consists of an average over 100–200 laser shots. The averaging is done by the computer which reads the ionizaton signal after every laser shot via a gated box-car averager (PAR model 162) operated in a linear mode.

The final-state distribution of the collisionally excited $l>2$ states at a fixed τ and Xe pressure is recorded by averaging the ionization signal using a gated box-car integrator as the ionization field is increased. If the gate into the box car is set wide (0.5 μs) to accept all the ionization signal, as shown in Fig. 6, the ion current at any field value E then represents a sum of all ions in the states that are

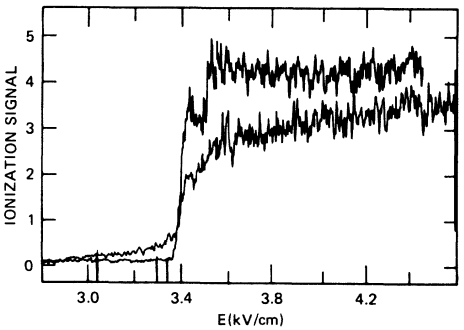

FIG. 6. Plot of the ion current as the field-ionization pulse amplitude is increased. The top curve was recorded with no xenon while the bottom curve resulted when xenon was introduced in the beam apparatus. Both signals were recorded 2 μs after the d states were excited by the laser pulses.

field ionized at a field $\leq E$. The number of ions field ionized in a field interval ΔE around E is then given by $(dI/dE)\Delta E$, where I is the ion signal.

The ionization signal can also be time resolved, by virtue of the fact that the ionization pulse increases in time (rise time=0.3 μs) and ionizes those states earlier that field ionize at lower fields. If the ionization signal is recorded with a very narrow gate (~ 50 ns) by a box car, then we can record the field-ionization signal coming from only those atoms which ionize at the peak of the field-ionization pulse. A plot of time-resolved signal of 18d state as the field is increased is shown in Fig. 7. The two partially resolved peaks at the lower field [Fig. 7(b)] are due to the ion signal from the $|m_l|=0$ and 1 component of the 18d state, whereas the third peak at higher-field results from collisionally populated diabatic states of $l \geq 2$.

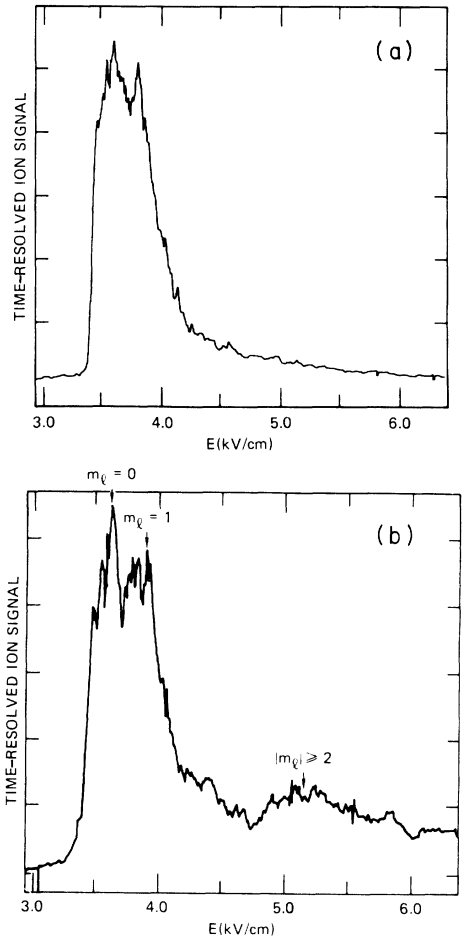

FIG. 7. Time-resolved ionizaton spectrum of Na atoms. A fixed narrow ~ 15 ns gate to the box-car averager time resolves the ionization signal, as the FI pulse amplitude is increased. In essence only the signal coming from the atoms which ionize at the peak of the ionization (rise time 0.3 μs) are recorded. In (a) the two partially resolved peaks correspond to the $|m_l|=0$ and 1 component of the 18d states. No other features are present since no xenon is present to redistribute the atoms to other l or $|m_l|$ states. The presence of Xe in (b) results in another feature at a higher field which corresponds to the collisional redistribution to higher l and $|m_l| \geq 2$ which ionize diabatically at higher fields. In recording these two plots a dc field of 13 V/cm and a Stark field of ~ 40 V/cm switched on 100 ns after the laser pulses were used. Similar plots were also recorded without any field.

III. RESULTS

A. Cross sections in zero field

The total l-mixing cross sections are obtained by fitting the fluorescence and the field-ionization data as a sum of two exponentials. As described above, the fast decay rate $k_+ = k_r + A_d$, obtained by varying the time delay τ and recording either the fluorescence or the integrated ionization current (see Fig. 5). When the fast decay rate k_+, measured at several Xe pressures is plotted versus Xe pressure, the slope of this graph provides the collisional-mixing rate and the intercept, the radiative decay rate A_d of the d states.[14] A typical plot of the fast collisional decay rate as a function of relative Xe pressure is shown in Fig. 8 for $n=23$.

As mentioned previously, the l-mixing cross sections $\sigma_{l\text{mix}}$ for $9 \leq n \leq 15$ were measured using fluorescence in a cell-type apparatus, and for $15 \leq n \leq 23$, we used an atomic beam apparatus with the SFI method. While the cell apparatus provided us with absolute values of cross section, the beam-type apparatus afforded us only the relative cross section as the Xe number density was not absolutely calibrated. Our measurement at $n=15$, with the cell and the beam apparatus, however, provides us a method of calibrating the relative cross sections obtained in the beam apparatus.

The l-mixing cross section $\sigma_{l\text{mix}}$ is shown plotted as a function of the principal quantum number n in Fig. 9 and is tabulated in Table I. The cross section increases from $n=9$ to $n=18$, rapidly at first, and then slowly reaches a maximum value at $n=18$. Beyond $n=18$, the cross section may exhibit a slow decrease. This n dependence of $\sigma_{l\text{mix}}$ is similar to that seen with He, Ne, and Ar, except that the cross sections due to Xe are an order of magnitude larger than those for Ar. Whereas the cross section for He, Ne, and Ar peaked at $n=10$–12, the peak for xenon is at a significantly higher n ($n=18$–19). The large l-mixing cross sections observed here and the peaking of the cross section at $n=18$ are not entirely surprising in the light of the models that have ex-

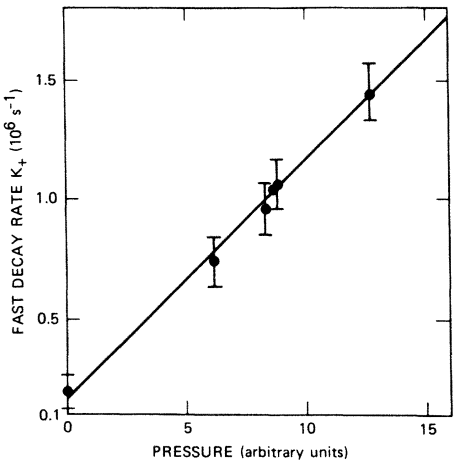

FIG. 8. Typical plot of the fast decay rate k_+ as a function of Xe pressure (arbitrary units). The slope of this curve provides the relative cross section for the $23d$ state.

plained previous measurements of the $\sigma_{l\text{mix}}$ due to other noble gases[4,5] and from the results of a similar measurement made on the nf states of Rb.[3] These models treat the Rydberg-atom—noble-gas-perturber interaction as collisions between the perturber and the quasifree Rydberg electron and the perturber—Na^+-core collision. For the l-mixing process with noble gases, the latter interaction can be neglected. The important parameter that describes the Na—noble-gas l-mixing process is the e^-—noble-gas scattering length L. The e^--Xe scattering length of $L=6.5a_0$ is the largest for any

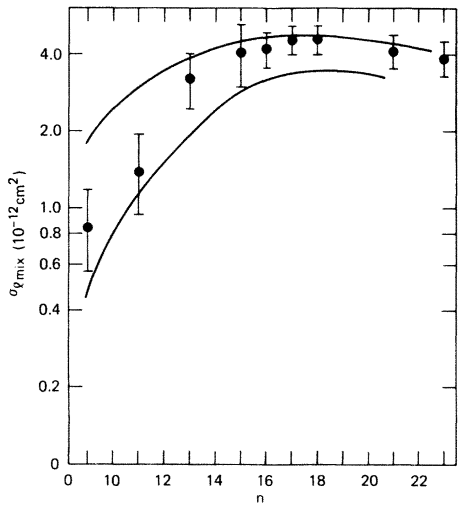

FIG. 9. Semilogarithmic plot of Xe l-mixing cross section versus n, the principal quantum number of the d state. The error bars represent the statistical uncertainty in our data. The upper and lower solid curves correspond to the maximum and minimum bound of the cross section calculated by de Prunelé and Pascale (see text).

TABLE I. Measured l-mixing cross section $\sigma_{l\text{mix}}$ of Na nd states with xenon. The numbers in parentheses represent the statistical uncertainty in our data.

n	$\sigma_{l\text{mix}}$ (10^3 Å^2)
9	8.65(3.0)
11	14.4(5.0)
13	32.4(8.0)
15	42.0(12.0)
16	42.4(6.0)
17	46.2(6.0)
18	46.4(6.0)
21	41.8(6.0)
23	39.0(6.0)

noble gas (compared to e^--Ar scattering length of $1.7a_0$). The cross section clearly scales as the scattering length of the e^-—noble-gas atom.

de Prunelé and Pascale have recently calculated the l-mixing cross section of the Na d state with various noble gases including xenon, using the semiclassical method.[10] The cross sections obtained from their calculations are also plotted in Fig. 9 as a solid curve, along with our results. The upper and lower dashed curves correspond to the maximum and minimum bound of the cross section, respectively. This calculation is based on the assumption that the electron-perturber interaction is short ranged compared to the size of the Rydberg atom. The upper and lower bounds of the calculated cross section result from particular orientations of the collision frame with respect to a fixed Rydberg-atom frame.[10] In the absence of any collisional symmetry (as is the case in our experiment), the cross section is obtained by averaging over all collision angles. The overall agreement between the calculated and the experimentally observed cross section is quite good.

B. Final-state distriution in zero field

A typical final-state distribution plot of the Rydberg states after collisions with Xe is shown in Fig. 6. A similar plot with no collisions is also shown in the same figure. In the absence of collisions the total ion signal remains constant as the field is increased beyond the $|m_l|=1$ threshold of the $18d$ state. However, in the presence of Xe, Fig. 6 shows that ion current keeps on increasing steadily beyond the $|m_l|=1$ threshold of the d state, until at a high-field value, the total ion signal is about 80—100% of that for the case with no collisions. This indicates that the loss in population in the d states, as evidenced by the reduction of $\sim 50\%$ in the step size of the d-step ion signal is balanced by the increase in population of states with $l>2$. In

fact, approximately 30% of the $l>2$ population is adiabatic ($|m_l| \leq 2$) and ~70% is diabatic ($|m_l| > 2$). This can be seen by comparing the size of the collision signal below the $m_l=0$ threshold and above the $|m_l|=1$ threshold of the 18d state. Similar final-state distribution for other states leads us to conclude that collisionally populated $l>2$ states are as likely to be in low-$|m_l|$ states ($|m_l| \leq 2$) as they are in numerous high-$|m_l|$ ($|m_l| > 2$) states. The appearance of collisionally populated $l>2$ diabatic states is also seen in the time-resolved final-state distribution of 18d state, as shown in Fig. 7(b). The third peak on the high-field end in Fig. 7(b), which is missing when no xenon is present [Fig. 7(a)] shows the presence of the diabatic states. Previous investigations have suggested that there is no Δl selection rule for the collisional l-mixing process.[2] This is in agreement with the notion that the l-mixing process is caused by a short-range interaction between the electron and the perturber. Our observations here suggests that most collisions end up with $|m_l|$ ($l \geq 2$) changing by 0—2 and very few with $\Delta|m_l| > 2$. We note that this observation of the final-state distribution with low-$|m_l|$ values is to be contrasted with the complete mixture of all possible $|m_l|$ states ($l \geq 2$) inferred at high rare-gas pressures (or at a long time after the exciting laser pulse at intermediate pressures) in previous cell measurements of the l-mixing cross sections.[1] These previous measurements indicate that the observed radiative lifetime of the collisionally populated states at high pressures (or long τ) are in very good agreement with the calculated average lifetime τ_{eff} of *all* $l \geq 2$ states of the same n for hydrogen.[1] Multiple collisions between the Na and rare-gas atoms (at high rare-gas pressure or long τ) may therefore result in a complete mixture of all $l \geq 2$ and $|m_l|$ states of same n. The single collision condition in our present beam experiment and the observation of final states with predominantly low $|m_l|$ suggest that a single collision changes $|m_l|$ mostly by 0—2, whereas no such selection is observed for Δl.[2] Since previous measurements of Na l-mixing with other rare gases shows a complete $|m_l|$ redistribution (for $l \geq 2$) at long τ, a change of $|m_l|$ mostly by 0—2 in a single collision suggests that several collisions (~5 for $n=15$) with rare-gas atoms may be required for a complete statistical redistribution of all final states of $l \geq 2$.

C. Cross sections in electric field

To investigate the effect of small electric fields on the l-mixing process, we measured the l-mixing collision cross section as well as the final-state distribution of the collisionally redistributed Na atoms for several nd states. The cross section $\sigma_{l\text{mix}}$ in the presence of the electric field was measured analogous to the zero-field case described earlier. To ensure that the laser pulses only excited the d states of Na, an electric field pulse was applied to the plates 50 ns after the laser excitation pulses. If instead a dc field were employed, it would tend to mix the d character into higher l states with the result that more than one l state would be excited. For $n=16$ and 23, the cross section $\sigma_{l\text{mix}}$ was only measured at fields of 100 and 12 V/cm, respectively (see Table II). The cross-section variation with increasing electric field was examined in some detail for the 18d state. As shown in Fig. 10, the cross section drops slowly to ~60% of its zero-field value as the field is increased to 50 V/cm and does not change at 100 V/cm. While the cross section of the 16d state also decreased to ~50% of its zero-field value at a field of 100 V/cm, no change in the cross section was observed for $n=23$ at fields of 12 V/cm.

D. Final-state distribution in electric field

Although a small electric field (50 V/cm for $n=18$) decreases the cross section by ~50%, its effect on the final state of the collisionally redistributed atoms is more noticeable. Figures 11 and 12 show a typical final-state distribution plot obtained by recording the ionization signal as the ionizer field is swept from low to high fields, at a fixed τ and Xe pressure. The effect of the electric field, as is evident from Figs. 11 and 12, is to reduce the number of atoms ending in the low-$|m_l|$ states ($|m_l| \leq 2$) of the manifold ($l>2$). A rough estimate shows that this reduction is of the order of 3—5.

To explain this modification in the collision process, as a result of a small field, we consider two important changes that occur in the atomic system. The first change is the energy-level shift or the Stark shift of the Rydberg atom, which affects both the

TABLE II. Relative l-mixing cross section $\sigma_{l\text{mix}}$ for the Na nd states in the presence of a small electric field.

	Electric field (V/cm)	Relative cross section
$n=16$	0	1.00
	100	0.60(0.10)
$n=18$	0	1.00
	30	0.85(0.10)
	50	0.64(0.10)
	100	0.63(0.10)
$n=23$	0	1.00
	12	1.00(0.10)

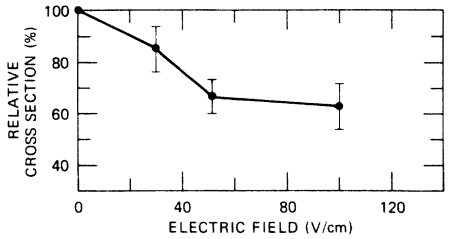

FIG. 10. Relative l-mixing cross section for the $18d$ state as the Stark (electric) field is increased.

initially excited d states and states of the same n but $l>2$. The second change is the strong spatial modification of the wave function.[16] To understand why such a spatial modification may result in a lower cross section or a modified final-state distribution, recall that the fields at which these changes take place, e.g., $V=50$ V/cm for $18d$, corresponds to the d states turning into linear Stark states (Fig. 13). This implies that the electronic wave function is localized on the $+\hat{z}$ (if the core is at the origin) or the $-\hat{z}$ side of the atom depending on the sign of the Stark shift (positive or negative). Here we have assumed that the electric field is along $\hat{z}$. Stark states of $l>2$, which have a maximum Stark shift, positive or negative are also strongly localized either on the $+\hat{z}$ or $-\hat{z}$ side of the atom, respectively. Similarly, states which lie in between are localized near the center, i.e., $z=0$. Since the l-mixing collision process is mediated by a very short-range interaction between the electron and the Xe atom, it is evident that spatial overlap between the initial and final state is important.

The Stark shift of the initial and final energy levels of the Rydberg atom and the consequent change in the energy spacing can also give rise to the change in l-mixing cross section. Previous measurements of $\sigma_{l\text{mix}}$ have indicated that the cross section for the collision mixing of the f states of Na into states of

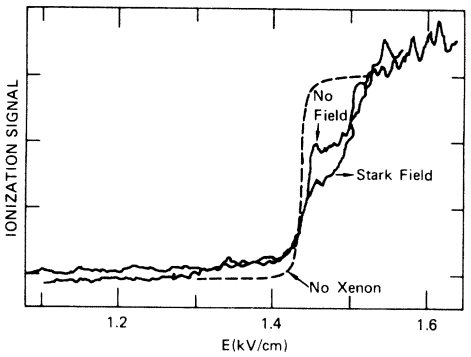

FIG. 12. Typical ion plot showing the reduction of the low-$|m_l|$ states of $l>2$ when a small electric field is applied at a fixed Xe pressure. The plots were recorded as indicated in the figure. The Stark field of 10 V/cm was applied for the indicated plot. The dashed line corresponds to no xenon being present (with no Stark field) and takes into account any blackbody-radiation–induced background. A similar dashed plot recorded in the present of a Stark field (not shown here) is similar except it is offset to the same extent as the solid traces are on the low-field end.

higher l is about equal to that for the d states.[2] Since $\Delta E=E_{nd}-E_{nf}$ is 10 times larger than $\Delta E=E_{ng}-E_{nf}$, it is tempting to conclude that the energy separation between the initial and final states is not important for the l-mixing process. However, as is well known, the cross section for $ns\rightarrow np$ collisional transfer is $\sim 10^2$ times smaller than the l-mixing process, because of the larger energy separation $\Delta E=E_{ns}-E_{np}$. Recently, Hickman[17] has calculated the cross section for the collision process $ns\rightarrow np$ as a function of the energy separation $\Delta E=E_{ns}-E_{np}$. This calculation is based on a model wave function using the approximate radial wave functions

$$F_{nl}(r)=N_{nl}r^{n-1}\exp[-r/(n-\delta_l)]\ ,$$

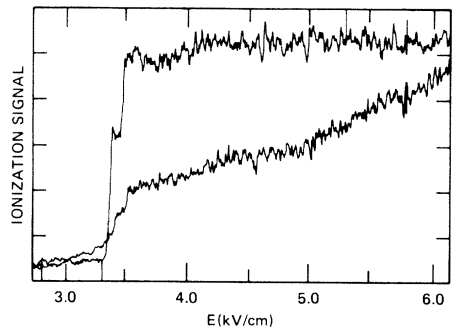

FIG. 11. Integrated ion current recorded 2.5 μs after the laser pulse. The top plot was recorded in the absence of Xe while the lower plot was recorded with Xe.

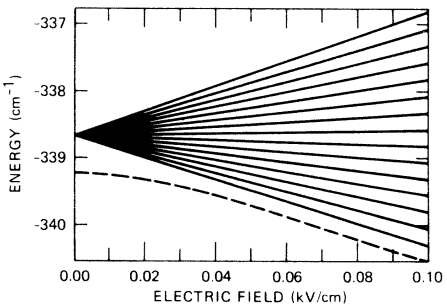

FIG. 13. Energy-level diagram of the Na $18d$ (dashed lines) and neighboring states of higher l (solid lines) as a function of the electric field. Note that $m=0$ for all states.

where N_{nl} is a normalizing constant and δ_l is the quantum defect of the n,l state. It is also assumed in this calculation that the electron rare-gas interaction can be approximated by

$$V(\vec{R}-\vec{r})=2\pi L\delta(\vec{R}-\vec{r}) ,$$

where $\vec{R}$ and $\vec{r}$ are the coordinates of the collision partner and the Rydberg electron, and L the electron–collision-partner scattering length (in atomic units). The calculations performed for n in the range $10 \leq n \leq 20$, show that if

$$\frac{n^2\Delta E}{hV_r} \sim 1 \text{ a.u.} ,$$

the transition cross section will be at least 90% of its value for $\Delta E=0$, i.e., if the initial and final states were truly degenerate.[17] If we assume a similar result for the l-mixing cross section as a function of the energy spacing in zero field we see that

$$\frac{n^2\Delta E}{hV_r} \sim 1 \text{ a.u.}$$

at $n=18$, implying that the states nd and nl are effectively degenerate.

To investigate the effect of the Stark shift on the l-mixing cross section, using the results of the model calculations outlined above, we neglect any alteration in the spatial overlap between the initial and the final state due to the electric field. Figure 13 shows the change in the energy-level spacing between the $18d-18l$ states, as the electric field is increased from 0 to 100 V/cm. At zero field

$$\Delta E=E_{18d}-E_{18f}\simeq 0.5 \text{ cm}^{-1}$$

and the levels $18d$ and $18l$ may be considered effectively degenerate for the collisional-mixing process. At fields of 50 V/cm, we see from Fig. 13 that the degeneracy approximation for the l mixing of the nd states is only approximately valid. The condition

$$d=\frac{n^2\Delta E}{hV_r} \sim 1$$

holds only for the lower four or five states of the Stark manifold. For the highest state in the Stark manifold $d \sim 2-3$ a.u., and consequently, these states are not effectively degenerate. The functional dependence of the partial l-mixing cross section $\sigma(nd \rightarrow nl)$ on the degeneracy parameter d depends on the choice of the wave function. For the collision process $np \rightarrow ns$, Hickman's calculations[17] show that if $d \sim 2-3$, the cross section drops to $\sim 70\%$ of its value at $d=0$. Although these calculations were not performed for the d-state mixing, it seems reasonable that some of the decrease in the cross section observed with the application of electric field may be attributed to change in the level splitting. Only detailed calculations taking into account both the energy-level effect and the spatial distortion of the wave functions can quantitatively account for the decrease in the collision cross sections and the final-state distribution of the collisionally populated states.

ACKNOWLEDGMENTS

This work was supported by the Air Force Office of Scientific Research under Contract No. F49620-79-C-0212. We are pleased to acknowledge useful discussions with R. F. Stebbings, F. B. Dunning, and A. P. Hickman in the course of this work.

*Present address: Centre d'Etudes Nucléaires de Saclay, Service de Physique des Atomes et des Surfaces, F-91191 Gif-sur-Yvette Cedex, France.

†Present address: Schlumberger-Doll Research, Ridgefield, Connecticut 06877.

‡Present address: Fakultät für Physik, 3 Herman Herder Strasse, D-7800 Freiburg, West Germany.

[1]T. F. Gallagher, S. A. Edelstein, and R. M. Hill, Phys. Rev. A 15, 1945 (1977).

[2]T. F. Gallagher, W. E. Cooke, and S. A. Edelstein, Phys. Rev. A 17, 904 (1978).

[3]M. Hugon, F. Gounand, P. R. Fournier, and J. Berlande, J. Phys. B 12, 2707 (1979).

[4]T. F. Gallagher, R. E. Olson, W. E. Cooke, S. A. Edelstein, and R. M. Hill, Phys. Rev. A 16, 441 (1977).

[5]K. A. Safinya and T. F. Gallagher, Phys. Rev. A 22, 1588 (1980).

[6]F. G. Kellert, C. Higgs, K. A. Smith, G. F. Hildebrandt, F. B. Dunning, and R. F. Stebbings, J. Chem. Phys. 72, 6312 (1980).

[7]C. Higgs, K. A. Smith, F. B. Dunning, and R. F. Stebbings, J. Chem. Phys. 75, 745 (1981).

[8]F. G. Kellert, T. H. Jeys, G. B. McMillian, K. A. Smith, F. B. Dunning, and R. F. Stebbings, Phys. Rev. A 23, 1127 (1981).

[9]J. I. Gersten, Phys. Rev. A 14, 1354 (1976); R. E. Olson, Phys. Rev. A 15, 631 (1977); A. Omont, J. Phys. (Paris) 38, 1343 (1977); A. P. Hickman, Phys. Rev. A 23, 87 (1981).

[10]E. Prunelé and J. Pascale, J. Phys. B 12, 2511 (1979).

[11]M. P. Slusher, C. Higgs, K. A. Smith, F. B. Dunning, and R. F. Stebbings, *Abstracts of the XII International Conference on the Physics of Electronic and Atomic Collisions, Gatlinburg, Tennessee, 1981,* edited by Sheldon

Datz (North-Holland, Amsterdam, 1981); F. Gounand, T. F. Gallagher, K. A. Safinya, and W. Sandner, *ibid.*

[12]M. G. Littman, M. I. Zimmerman, and D. Kleppner, Phys. Rev. Lett. 37, 486 (1976).

[13]T. F. Gallagher, L. M. Humphrey, W. E. Cooke, R. M. Hill, and S. A. Edelstein, Phys. Rev. A 16, 1098 (1977).

[14]The pressure-independent coefficients A_d also includes $\sim 20\%$ contribution (for $n=18$ states) from the blackbody-radiation—induced redistribution of the initially populated *nd* state. See T. F. Gallagher and W. E. Cooke, Phys. Rev. Lett. 42, 835 (1979).

[15]T. H. Jeys, G. W. Foltz, K. A. Smith, E. J. Beiting, F. G. Kellert, F. B. Dunning, and R. F. Stebbings, Phys. Rev. Lett. 44, 390 (1980).

[16]H. E. Bethe and A. Salpeter, *Quantum Mechanics of One- and Two-Electron Atoms* (Academic, New York, 1957).

[17]A. P. Hickman, Phys. Rev. A 19, 994 (1979).